

## Interaction of stopped antiprotons with copper

J. Jastrzębski, W. Kurcewicz, P. Lubiński, A. Grabowska, and A. Stolarz  
*Heavy Ion Laboratory and Institute of Experimental Physics, Warsaw University, 02-097 Warsaw, Poland*

H. Daniel, T. von Egidy, F. J. Hartmann, P. Hofmann, and Y. S. Kim  
*Physik-Department, Technische Universität München, D-8046 Garching, Germany*

A. S. Botvina, Ye. S. Golubeva, and A. S. Iljinov  
*Institute for Nuclear Research, Russian Academy of Sciences, 117312 Moscow, Russia*

G. Riepe  
*Forschungszentrum Jülich, D-5170 Jülich, Germany*

H. S. Plendl  
*Florida State University, Tallahassee, Florida 32306*  
(Received 9 March 1992)

A natural Cu target was irradiated with the antiproton beam from the Low Energy Antiproton Ring facility at CERN. The 105 MeV/c  $\bar{p}$  beam was completely slowed down inside a thick target producing many radioactive products. Starting shortly after the irradiation and continuing for about one year, this residual activity was counted using off-line gamma-ray spectroscopy techniques. The yields of 40 radioactive reaction products were determined. The charge dispersion and complete mass yield distribution were deduced using a well-established fitting procedure. The shape of the mass yield and, in particular, the average number of removed nucleons, the dispersion of the mass distribution, and its logarithmic slope characterize the average energy deposited during the antiproton-nucleus interaction. We compare these quantities with similar data gathered for other projectiles interacting with natural Cu targets. These comparisons indicate that the average excitation energy of the system formed after the stopped antiproton annihilation is similar to the average excitation energy following 2-GeV proton interaction with Cu nuclei. The observed mass distribution is also compared with the intranuclear cascade calculations.

PACS number(s): 25.43.+t

### I. INTRODUCTION

For a number of years, the interaction of antiprotons with nuclei has been considered as a process in which new phenomena may perhaps be observed. The most exotic of them, such as the formation of a quark-gluon plasma and nuclear explosions, are expected only for a tiny fraction of energetic antiproton interactions with nuclei, when after a central collision the antiproton annihilates deeply inside the nuclear volume [1,2]. However, already the interaction of stopped antiprotons with nuclei may create reaction products with characteristics quite different than observed after more conventional nuclear reactions induced by light or heavy ions [3–5]. These conjectures are based on the fact that during the annihilation of an antiproton on the nuclear surface a substantial amount of energy is released in the nucleus in a more uniform way (without the impact parameter dependence) than during energetic proton or heavy-ion excitation. Also, the linear and angular momenta of the reaction products are not the result of a transfer from the projectile, but are rather determined by the angular momentum of the last antiprotonic orbit and by the recoil, following particle emission.

After the annihilation of a stopped antiproton on the

nuclear surface, a fraction of the created particles (mainly pions) enters the nuclear volume and initiates an intranuclear cascade. Some fast nucleons are promptly emitted, and the remaining part of the absorbed annihilation energy heats the nucleus so that it evaporates nucleons, heavier clusters, or fissions. As in the usual deep spallation or fission processes, heavy reaction residues are formed and can be detected using classical radiochemical methods. The charge and mass distribution of these residues carry information on the energy deposition process during the antiproton-nucleus interaction.

The radiochemical investigation of heavy reaction residues after stopped antiproton annihilation on nuclei has recently been carried out by some of us [6–8]. Targets of  $^{92,95,98}\text{Mo}$ ,  $^{\text{nat}}\text{Ba}$ , and  $^{165}\text{Ho}$  were irradiated with antiprotons from the Low Energy Antiproton Ring (LEAR) facility at CERN. From the gamma-ray intensities of the radioactive reaction products, mass yield distributions were deduced and compared with the intranuclear cascade plus evaporation model [3]. The excellent agreement obtained seems to indicate that the model used correctly describes the magnitude and distribution of the excitation energy deposited in the target nuclei during the antiproton-nucleus interaction.

In the present work, the investigation of the interac-

tion of stopped antiprotons with nuclei is extended to a  $^{nat}\text{Cu}$  target. Such an extension is motivated for a number of reasons. First, we wish to establish the systematics of the antiproton-nucleus interaction in a large target mass range, and the present paper is the next step toward this goal. Second, we wish to check if the previously used intranuclear cascade plus evaporation model can do as well in another mass region in the description of heavy reaction residues. And, last but not least, an investigation of the antiproton interaction with  $^{nat}\text{Cu}$  should allow a comparison with the results obtained using the same target and a variety of projectiles such as protons and helium ions [9–14], heavy ions [10,11,15–25], pions [13,26,27], and gamma rays [28].

## II. EXPERIMENTAL TECHNIQUE AND RESULTS

Natural Cu targets of purity better than 99.99% were irradiated with an antiproton beam from the LEAR facility at CERN. Before impinging on the Cu foils, the 105 MeV/c  $\bar{p}$  beam passed through a 18.5 mg/cm<sup>2</sup> beryllium window, 2 cm of air, and a 3.6 mg/cm<sup>2</sup> Mylar support. At that point, the beam energy was 4.2 MeV. Two Cu targets were independently irradiated. The first target was composed of a stack of six Cu foils of thickness (beginning from the beam side) 10.4, 19.3, 40.8, 19.5, 10.5, and 85 mg/cm<sup>2</sup>. This stack was irradiated by two antiproton “spills” of 10 min duration each, with a 20 min time lapse between them. The total number of antiprotons impinging on this target was about  $4.5 \times 10^8$ . The second target was composed of two 40.6 mg/cm<sup>2</sup> copper foils and was irradiated by one spill of 15 min duration with approximately  $3.5 \times 10^8$  antiprotons. As there was no direct antiproton counting device in front of the target, the numbers of antiprotons quoted above were estimated from the experimentally determined mass yield curve (see below) using the assumption that the annihilation of each antiproton leads to the formation of one heavy reaction residue.

The off-line gamma-ray counting for the first target started 40 min after the end of irradiation and for the second target 6 min after the end of irradiation. A Pb-shielded HPGe detector with 19% efficiency and 1.9 keV resolution (for  $^{60}\text{Co}$ ) was used for the gamma-ray counting at CERN for a period of about 2 days for each target. Later, the samples were counted in Warsaw for a period of about 1 year using two HPGe detectors of 15% and 42% efficiency, respectively. The energy resolution of these detectors for  $^{60}\text{Co}$  gamma rays was 1.8 and 1.95 keV, respectively.

Separate counting of the foils that made up the first target showed an activity only in the central foil of 40.8 mg/cm<sup>2</sup> thickness. This gives an upper limit to the spread in the beam range inside the target as well as for the contamination of our results by secondary reactions. For all investigated cases, the contribution of other reactions is smaller than the quoted experimental error in the intensities of residues.

The resulting gamma-ray spectra have been analyzed with the computer program ACTIV [29]. The identification of the radioactive nuclei and the activity

determination were based on known decay data [10,30,31].

From the measured activities, the total number of produced radioactive atoms during the antiproton irradiation was deduced for each isotope. A delta-function spill shape was assumed for isotopes with half-lives longer than 5 h. This assumption introduces an error smaller than 1% for the yield of these isotopes. For shorter-lived isotopes, a correction for the spill shape (fast rising of the antiproton beam and its slow, exponential decay) was applied. The “average” spill shape was determined in another experiment with an antiproton counter telescope.

Table I presents the yields of the radioactive products observed in the  $\bar{p} + ^{nat}\text{Cu}$  interaction. The units in this table are the numbers of atoms produced per 1000 stopped antiprotons, which were determined by the procedure described above.

Recently, taking the opportunity of another experiment, a thick Cu target was again irradiated by the antiproton beam, this time using direct antiproton counting as described, e.g., in Ref. [32]. The intensities of the most intense gamma-ray transitions observed after this irradiation were used to check the previous normalization of the isotope yield. On the average, the new yield was found to be a factor of  $1.2 \pm 0.3$  lower than obtained from the previous determination (the quoted uncertainty includes statistical as well as estimated systematic errors). Taking into account the quoted errors, no renormalization of the data presented in Table I was attempted.

## III. DATA ANALYSIS

From the yields of the radioactive reaction products, the charge dispersion and complete mass distribution were deduced. The procedure followed was described in detail recently [25], and we refer to this reference for bibliography and the discussion of the method used. Here, for completeness, we present the formulas which gave the best fit for the antiproton on  $^{nat}\text{Cu}$  data. The fitted function was of the form

$$\sigma(A, Z) = Y(A)P(Z - Z_p), \quad (1)$$

where  $A$  and  $Z$  are the mass and charge of the product, respectively, and

$$Y(A) = \exp(\alpha_0 + \alpha_1 A + \alpha_2 A^2 + \alpha_3 A^3), \quad (2)$$

$$P(Z - Z_p) = C \exp[-(Z - Z_p)^2 / (2\alpha_4)], \quad (3)$$

$$Z_p = \alpha_5 + \alpha_6 A, \quad (4)$$

$$C = (2\pi\alpha_4)^{-1/2}. \quad (5)$$

The seven parameters  $\alpha_0 - \alpha_6$  were simultaneously fitted to 37 of experimentally determined isotope yields. After the fitting procedure, the total yield for each mass was obtained from the partial experimental yield using formula (1).

Figure 1(a) gives the deduced charge dispersion curve for the reaction  $\bar{p} + ^{nat}\text{Cu}$ , and Fig. 2(a) presents the mass yields for the same reaction. In Figs. 1(b) and 2(b) are shown similar data for the reaction of 3.9 GeV protons with a natural Cu target. The proton results were ob-

tained from the cross sections determined in Ref. [10], using for consistency the same fitting procedure as employed for our antiproton data.

The similarity of the charge dispersion curves is evident from Fig. 1. Their widths are almost identical [full width at half maximum (FWHM)= $1.45\pm 0.02$  and  $1.41\pm 0.02$  for antiprotons and protons, respectively] and correspond to the width observed in the  $^{20}\text{Ne} + \text{natCu}$  reaction at a bombarding energy above 50 MeV/nucleon [25]. The mass yields are also very similar, although a larger scattering of the antiproton data is observed. (Additional comparisons of the antiproton mass distribution

with distributions gathered in other reactions are presented in the following section.)

Using the fitted mass distribution [Eq. (2)], the average number of nucleons removed from the target was calculated. This number depends slightly on the mass range used for the calculations. Keeping in mind arguments presented in Ref. [25], we have calculated this average value for masses between  $A=25$  and the target mass minus 1. The result is

$$\langle \Delta A \rangle = (A_{\text{targ}} - 1) - \langle A_{\text{prod}} \rangle = 12.6 \pm 0.6,$$

where

TABLE I. Yields of products of the type *C* (cumulative) or *I* (independent) from stopped antiproton interaction with  $\text{natCu}$ .

Product	Half-life	Experiment $N/1000 \bar{p}$	Type	Theory	
				Version 1 <sup>a</sup> $N/1000 \bar{p}$	Version 2 <sup>a</sup> $N/1000 \bar{p}$
$^{62}\text{Zn}$	9.3 h	< 0.9	<i>I</i>		
$^{64}\text{Cu}$	12.7 h	$24.9\pm 4.3$	<i>I</i>	16.2	17.8
$^{61}\text{Cu}$	3.4 h	$9.7\pm 0.6$	<i>I</i>	6.0	5.6
$^{60}\text{Cu}$	24.4 min	$1.6\pm 0.1$	<i>I</i>	1.9	2.1
$^{57}\text{Ni}$	35.7 h	$0.86\pm 0.17$	<i>C</i>	0.1	0.3
$^{61}\text{Co}$	1.7 h	$6.6\pm 0.3$	<i>C</i>	7.5	5.4
$^{60}\text{Co}$	5.3 yr	$13.7\pm 0.9$	<i>C</i>	11.9	11.8
$^{58}\text{Co}$	70.9 d	$22.3\pm 0.9$	<i>I</i>	24.7	26.9
$^{57}\text{Co}$	272 d	$23.1\pm 1.4$	<i>I</i>	12.7	12.4
$^{56}\text{Co}$	77.1 d	$7.4\pm 1.4$	<i>C</i>	3.6	2.8
$^{55}\text{Co}$	17.5 h	$1.3\pm 0.2$	<i>C</i>	0.3	0.6
$^{59}\text{Fe}$	44.5 d	$2.2\pm 0.3$	<i>C</i>	4.2	4.7
$^{53}\text{Fe}$	8.5 min	$1.8\pm 0.3$	<i>C</i>	1.2	0.6
$^{52}\text{Fe}$	8.3 h	$0.26\pm 0.06$	<i>C</i>		
$^{56}\text{Mn}$	2.6 h	$3.8\pm 0.6$	<i>I</i>	6.4	4.8
$^{54}\text{Mn}$	312 d	$35.7\pm 2.0$	<i>I</i>	28.4	30.1
$^{52}\text{Mn}^m$	21 min	$2.8\pm 0.3$	<i>I</i> }		
$^{52}\text{Mn}$	5.6 d	$8.6\pm 0.6$	<i>I</i> }	10.8	9.9
$^{56}\text{Cr}$	5.5 min	$0.49\pm 0.14$	<i>C</i>	0.3	0.2
$^{51}\text{Cr}$	27.7 d	$25.4\pm 1.4$	<i>C</i>	31.3	31.6
$^{49}\text{Cr}$	42.3 min	$4.9\pm 0.6$	<i>C</i>	2.1	1.7
$^{48}\text{Cr}$	21.6 h	$0.54\pm 0.09$	<i>C</i>		
$^{48}\text{V}$	16 d	$12.6\pm 0.9$	<i>I</i>	17.4	16.9
$^{48}\text{Sc}$	43.7 h	$1.2\pm 0.1$	<i>I</i>	0.8	1.2
$^{47}\text{Sc}$	3.4 d	$5.1\pm 0.6$	<i>I</i>	3.8	4.5
$^{46}\text{Sc}$	83.8 d	$9.7\pm 0.9$	<i>I</i>	15.0	13.9
$^{44}\text{Sc}^m$	2.4 d	$7.4\pm 0.6$	<i>I</i> }		
$^{44}\text{Sc}$	3.9 h	$5.7\pm 0.6$	<i>I</i> }	18.7	19.9
$^{43}\text{Sc}$	3.9 h	$4.6\pm 0.6$	<i>C</i>	1.9	3.2
$^{47}\text{Ca}$	4.5 d	$0.31\pm 0.09$	<i>C</i>	0.1	0.1
$^{43}\text{K}$	22.3 h	$2.1\pm 0.2$	<i>C</i>	1.3	1.5
$^{42}\text{K}$	12.4 h	$4.6\pm 0.6$	<i>I</i>	5.2	7.3
$^{41}\text{Ar}$	1.8 h	$1.1\pm 0.1$	<i>C</i>	0.5	0.6
$^{39}\text{Cl}$	56 min	$0.74\pm 0.11$	<i>C</i>	0.8	0.4
$^{38}\text{Cl}$	37 min	$2.1\pm 0.3$	<i>C</i>	0.8	2.4
$^{38}\text{S}$	2.8 h	$0.14\pm 0.11$	<i>C</i>		
$^{29}\text{Al}$	6.6 min	$1.3\pm 0.2$	<i>C</i>	1.3	1.0
$^{28}\text{Mg}$	20.9 h	$0.23\pm 0.09$	<i>C</i>		
$^{27}\text{Mg}$	9.5 min	$0.91\pm 0.20$	<i>C</i>	0.7	1.3
$^{24}\text{Na}$	15 h	$1.9\pm 0.2$	<i>C</i>	4.7	1.5
$^{22}\text{Na}$	2.6 yr	< 1.9	<i>C</i>	5.7	2.9
$^7\text{Be}$	53.3 d	$7.4\pm 2.3$	<i>I</i>	22.2	7.1

<sup>a</sup>See text.

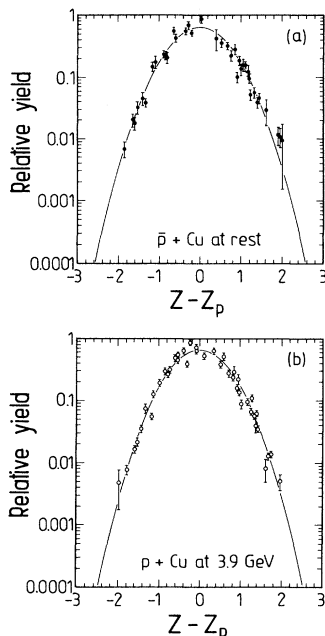


FIG. 1. Charge distribution deduced from the experimentally determined cross sections of the radioactive reaction products. (a) stopped  $\bar{p} + {}^{\text{nat}}\text{Cu}$  (present work) and (b)  $p + {}^{\text{nat}}\text{Cu}$  at 3.9 GeV bombarding energy (from Ref. [10]).

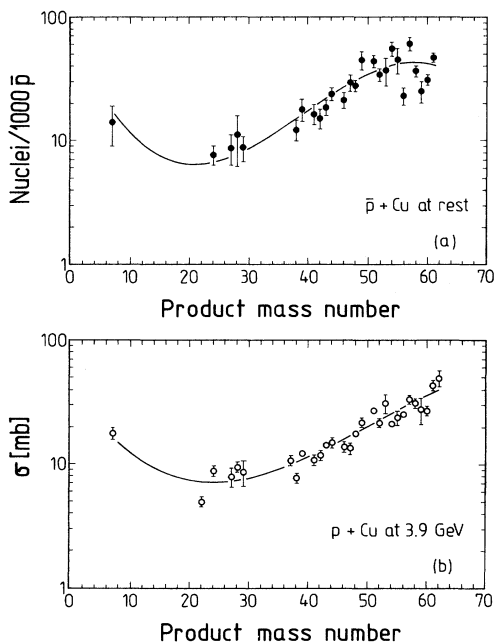


FIG. 2. Mass yields for the production of reaction residues in (a) stopped  $\bar{p} + {}^{\text{nat}}\text{Cu}$  and (b)  $p + {}^{\text{nat}}\text{Cu}$  at 3.9 GeV deduced from the experimentally determined cross sections of the radioactive products. The lines represent the global fit to all experimental cross sections [see Eq. (2)]. For  $\bar{p} + {}^{\text{nat}}\text{Cu}$  reactions, the fitted parameters are  $\alpha_0 = 3.916$ ,  $\alpha_1 = -0.2703$ ,  $\alpha_2 = 0.0088$ ,  $\alpha_3 = -0.745 \times 10^{-4}$ ,  $\alpha_4 = -1.319$ ,  $\alpha_5 = 1.321$ , and  $\alpha_6 = 0.4391$ .

$$\langle A_{\text{prod}} \rangle = \frac{\sum Y(A) A}{\sum Y(A)} .$$

Assuming now that, on the average, the evaporation of 1 mass unit in this mass region decreases the excitation energy of the thermalized reaction product by 9.7 MeV [33], the above  $\langle \Delta A \rangle$  value gives an upper limit of the average excitation energy  $\langle E^* \rangle$ , of about 120 MeV. In order to get a value rather than a limit, the number of nucleons emitted in the fast reaction phase has to be estimated. If during this phase on the average, e.g.,  $4 \pm 2$  nucleons are emitted [34,35], the average thermal excitation energy left in the reaction product would be  $1.4 \pm 0.3$  MeV/nucleon. However, as the mean energy carried away per emitted particle is temperature dependent, this value may be underestimated by as much as 10–20%. Indeed, the estimate of Ref. [33] was derived from experimental measurements of compound nuclei with much lower temperatures than observed after the antiproton annihilation.

Before ending this section, it is worth making some comments concerning the individual isotope yield. In the present investigation, we were looking for, but were unable to identify, the charge-exchange reactions [7], producing nuclei with proton number larger than target  $Z$ . Table I gives only an upper limit for the production of  ${}^{62}\text{Zn}$ .

Taking into account the target composition, the yield of  ${}^{64}\text{Cu}$  is the strongest from all produced species ( ${}^{64}\text{Cu}$  can only be formed from  ${}^{65}\text{Cu}$ , 31% in a natural Cu target). It is expected [7,34] that to produce this isotope the antiproton annihilates on a neutron in a far periphery of the nucleus. After the annihilation all produced pions miss the nucleus and the product is left with an excitation energy lower than the nucleon binding energy.

The production of light nuclei such as Be and Na can, at least partly, be a result of the fast multifragmentation of very hot target nuclei [36–38] or slow heavy-cluster evaporation [39]. The relative yield of these light nuclei in stopped-antiproton-induced reactions is similar although slightly smaller than in reactions with energetic protons. A suspicious lack of  ${}^{22}\text{Na}$  in the antiproton spectra is not well understood. An ultralow background experiment is in preparation to search again for this product in our Cu samples.

From the intranuclear cascade model calculations [3,40], it is expected that, because of the energetic particle emission, the nuclei produced after antiproton annihilation are left with rather high angular momenta (in the case of the Cu target, up to  $30\hbar$ ). The yield ratio of high- and low-spin isomers of the same product is a signature of a high angular momentum. Two analyzable cases are present in the  $\bar{p}$  data on the  ${}^{\text{nat}}\text{Cu}$  target: the  ${}^{52}\text{Mn}$  and  ${}^{44}\text{Sc}$  isotopes, both of them having isomers with spin-parity  $6^+$  and  $2^+$ . Their  $6^+/2^+$  isomeric ratios are shown in Table II, where a comparison with other reactions is also made. As seen, the  $6^+/2^+$  antiproton results are similar to those observed in low-momentum-transfer reactions (gammas, protons,  $\pi^-$ , energetic heavy ions) and are much smaller than in the intermediate-energy heavy-ion reactions.

At first glance the higher isomeric ratio for  ${}^{52}\text{Mn}$  than

TABLE II. Examples of isomeric ratios in nuclear reactions with  $^{nat}\text{Cu}$ .

Projectile	Energy	$^{44}\text{Sc}^m / ^{44}\text{Sc}$ ( $6^+ / 2^+$ )	$^{52}\text{Mn}^m / ^{52}\text{Mn}$ ( $6^+ / 2^+$ )	Ref.
$\gamma$	310 MeV	1.09±0.35		[28]
$\gamma$	600 MeV	1.12±0.12		[28]
$\gamma$	1000 MeV	1.23±0.14		[28]
$p$	3.9 GeV	1.18±0.07	a	[10]
$p$	28 GeV	1.24±0.03	4.27±0.12	[11]
$\bar{p}$	at rest	1.30±0.17	3.07±0.36	this work
$\pi^-$	0.5 GeV	1.25±0.05	1.41±0.63	[26]
$\pi^-$	1.5 GeV	1.53±0.10		[26]
$^3\text{He}$	350 MeV	1.51±0.21		[14]
$^3\text{He}$	910 MeV	2.08±0.29		[14]
$^{12}\text{C}$	25 GeV	1.20±0.09		[11]
$^{40}\text{Ar}$	80 GeV	1.40±0.30		[15]
$^{14}\text{N}$	3.9 GeV	1.44±0.09		[10]
$^{12}\text{C}$	45 MeV/nucleon	2.26±0.42	5.97±0.88	[24]
$^{12}\text{C}$	35 MeV/nucleon	3.39±0.48	8.02±1.10	[23]
$^{12}\text{C}$	25 MeV/nucleon	3.93±0.57	10.37±1.31	[24]
$^{20}\text{Ne}$	29.2 MeV/nucleon	2.68±0.23		[25]
$^{20}\text{Ne}$	22.7 MeV/nucleon	3.88±0.54		[25]
$^{20}\text{Ne}$	14.3 MeV/nucleon	5.43±3.22		[25]

<sup>a</sup>This isomeric ratio is not quoted; we believe that the cross section of  $^{52}\text{Mn}^m$  reported in Ref. [10] is a misprint.

for  $^{44}\text{Sc}$  seems to contradict the cascade results of Ref. [3], which predict that the average spin of the reaction residues increases monotonously with the number  $\Delta A$  of removed nucleons. It should be pointed out, however, that there are three components of the nuclear angular momentum [see relation (16) in Ref. [3]]: the antiproton orbital momentum in the atom state from which the absorption takes place and two sums of the angular momenta carried away by cascade particles and evaporation particles. In the case of the antiproton absorption by medium-weight nuclei, the value of the orbital momentum equals approximately  $(4-6)\hbar$  and the sum of the angular momenta carried away by the evaporation particles can reach a similar value. So, in order to eliminate these parts of the nuclear angular momentum and to investigate the angular momentum caused by the energetic particle emission, one needs to select isomers with spins higher than studied here (as it was done in  $\pi^-$  absorption studies [41] where isomers with spins up to  $20\hbar$  were investigated).

#### IV. DISCUSSION

##### A. Stopped antiproton annihilation compared to light-projectile-induced reactions

As discussed in a number of papers (see Ref. [25] for details and references), the shape of the mass distribution of heavy reaction residues is related to the average energy deposition in the reaction. With the increase in the deposited excitation energy, more particles are evaporated from the prefragment formed in the fast reaction phase, the mass distribution becomes broader and flatter, the average removed mass increases, and the logarithmic

slope [15] of the mass yield decreases. In the present work, the logarithmic slope of the mass yield  $k$  was determined by fitting the mass yield over the mass region between  $A_{\min}$  and  $A_{\max}$  with an exponential of the form  $Y(A) = C \exp(kA)$ . The  $A_{\min}$  and  $A_{\max}$  values were selected individually for each reaction (see below) as the limits of the observed exponential region.

The  $\langle \Delta A \rangle$  and  $k$  quantities were previously extensively studied for the  $^{nat}\text{Cu}$  target. The dependence of the logarithmic slope and  $\langle \Delta A \rangle$  on the projectile energy [15,25,42] indicates that for light and heavy projectiles these observables are almost independent of the projectile mass. There is, however, a strong dependence on projectile kinetic energy up to a bombarding energy of about 1–2 GeV. Above this energy the logarithmic slope and  $\langle \Delta A \rangle$  almost stabilize, indicating that the transferred excitation energy approaches its maximum value. (Therefore the 3.9-GeV proton data shown in Figs. 1 and 2 may be considered as representative for the limiting excitation energy transfer using “normal” projectiles.)

In Table III the parameters of the mass distributions resulting from the interaction of pions and protons with a natural copper target are compared with the present antiproton data. These parameters were deduced from the originally determined yields or cross sections using, for consistency, the fitting procedure described in Sec. III.

In many investigated cases, the logarithmic slope depends slightly on the selection of the mass region in which the slope is fitted. Therefore we also introduce in Table III a more objective parameter, the mass dispersion

$$\sigma_A = [\sum (\langle A_{\text{prod}} \rangle - A)^2 Y(A) / \sum Y(A)]^{1/2},$$

to account for the differences between shapes of the mass yields. The mass dispersion is calculated using the fitted

TABLE III. Parameters of the mass yield curve resulting from the interaction of light projectiles with Cu.

Projectile	Energy (GeV)	Average mass	Average	Dispersion of	Logarithmic slope		Ref.
		of the product $\langle A \rangle$ (u)	removed mass $\langle \Delta A \rangle$ (u)	the mass yield $\sigma_A$ (u)	$k$ (%)	$A_{\min}/A_{\max}$	
$\pi^-$	at rest	$60.1 \pm 0.5$	3.9	$3.2 \pm 0.2$	$65.8 \pm 3.4$	41/52	[27]
$\pi^+$	0.05	$56.4 \pm 0.2$	7.6	$3.8 \pm 0.1$	$24.3 \pm 2.3$	47/58	[13]
$\pi^-$	0.05	$57.0 \pm 0.2$	7.0	$4.0 \pm 0.1$	$33.6 \pm 4.1$	47/55	[13]
$p$	0.20	$58.6 \pm 0.5$	6.4	$4.0 \pm 0.2$	$33.6 \pm 1.7$	44/55	[13]
$\pi^-$	0.10	$57.8 \pm 0.5$	6.2	$4.6 \pm 0.2$	$28.6 \pm 2.0$	43/55	[13]
$\pi^+$	0.10	$57.2 \pm 0.4$	6.8	$4.9 \pm 0.2$	$25.5 \pm 2.7$	44/55	[13]
$p$	0.35	$57.3 \pm 0.5$	7.7	$5.2 \pm 0.2$	$24.2 \pm 2.7$	41/52	[13]
$\pi^+$	0.19	$56.8 \pm 0.5$	7.2	$5.2 \pm 0.2$	$18.9 \pm 3.1$	43/55	[13]
$\pi^-$	0.19	$57.3 \pm 0.5$	6.7	$5.3 \pm 0.2$	$20.7 \pm 2.0$	41/55	[13]
$p$	0.59	$55.7 \pm 0.5$	9.3	$6.1 \pm 0.2$	$18.3 \pm 1.7$	41/52	[12]
$\pi^-$	0.35	$55.8 \pm 0.5$	8.2	$6.3 \pm 0.2$	$16.2 \pm 2.4$	40/53	[13]
$\pi^+$	0.35	$55.1 \pm 0.5$	8.9	$6.6 \pm 0.2$	$13.8 \pm 2.4$	40/53	[13]
$\pi^-$	0.50	$52.8 \pm 0.5$	11.2	$8.1 \pm 0.2$	$11.9 \pm 0.8$	26/52	[26]
$\bar{p}$	at rest	$50.4 \pm 0.6$	12.6	$9.8 \pm 0.2$	$9.2 \pm 1.6$	41/52	this work
$\pi^-$	1.57	$51.1 \pm 0.8$	12.9	$10.4 \pm 0.2$	$4.7 \pm 0.5$	20/58	[26]
$p$	3.90	$50.8 \pm 0.8$	14.2	$10.6 \pm 0.2$	$5.6 \pm 0.3$	36/59	[10]
$p$	28.00	$50.3 \pm 1.0$	14.7	$11.2 \pm 0.2$	$5.0 \pm 0.3$	39/59	[11]

values of the mass distribution in the same mass region as it was taken for the calculation of the  $\langle \Delta A \rangle$  quantity ( $A=25$  and the target mass minus 1). Its increase accounts for the flattening of this distribution; i.e., it is the signature of the increasing average energy deposition. Figure 3 shows the dependence of  $\langle \Delta A \rangle$  and  $\sigma_A$  on the projectile bombarding energy.

The data of Table III and Fig. 3 allow us to compare the effectiveness of the antiproton energy transfer with that of light projectiles. We conclude that, on the average, the stopped antiproton annihilation imparts to the copper nuclei an amount of excitation energy comparable to that imparted by a proton of about 2 GeV incident energy.

### B. Antiproton mass removal as a function of target mass

Previously [6–8], the mass distribution for the interaction of stopped antiprotons with Mo, Ba, and Ho targets was determined by the same techniques as employed in the present work. The average number of nucleons removed from the copper target can therefore be compared with the values gathered for heavier targets. This comparison is shown in Fig. 4. If the average number of nucleons removed is plotted as a function of the target mass to the power  $\frac{2}{3}$ , a linear relationship is obtained for Cu, Mo, and Ho nuclei. On the other hand, the average number of nucleons removed from the Ba target is about 6 mass units lower than expected from the systematics of other targets.

### C. Product yield from the intranuclear cascade calculations

As in previous investigations of the stopped antiproton interaction with nuclei [6–8], the experimental data gathered in the present work were compared with intranu-

clear cascade (INC) calculations. These calculations were carried out using the model of nuclear absorption of stopped antiprotons [3]. According to this model, the antiproton annihilates at the beginning of the reaction on the surface of the nucleus, and a few pions (from two to

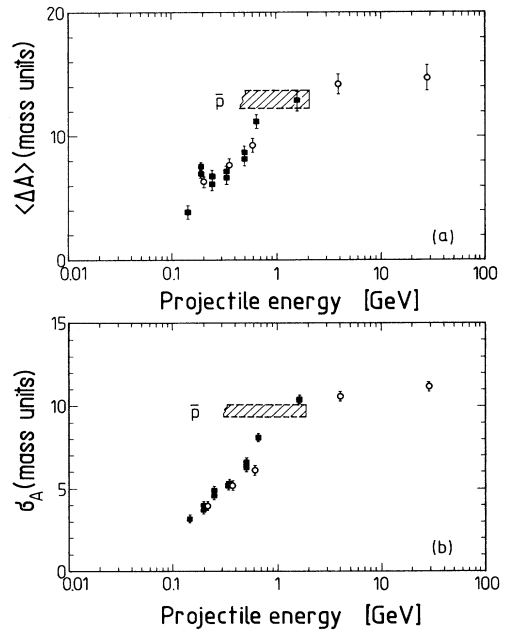


FIG. 3. (a) Average number of removed nucleons,  $\langle \Delta A \rangle$ , and (b) average dispersion of the mass distribution,  $\sigma_A$ , for pions (solid squares) and protons (open circles) interacting with a  $^{nat}\text{Cu}$  target. Data are plotted as a function of kinetic energy for protons and kinetic energy plus rest mass [26] for pions. The hatched corridors correspond to (a)  $\langle \Delta A \rangle$  and (b)  $\sigma_A$  for stopped antiprotons interacting with a  $^{nat}\text{Cu}$  target.

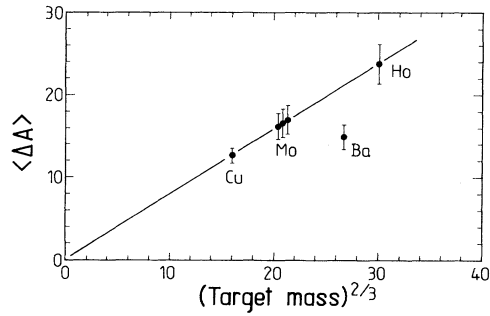


FIG. 4. Average number of removed nucleons after annihilation,  $\langle \Delta A \rangle = (A_{\text{targ}} - 1) - \langle A_{\text{prod}} \rangle$ , as a function of target mass to  $\frac{2}{3}$  power for stopped antiprotons. The Ho, Mo, and Ba data are from Refs. [7,8].

eight) are produced. Then the pions generate a cascade of sequential two-body collisions with nucleons within the nucleus. High-energy products of these collisions (nucleons, pions, etc.) escape from the nucleus, while low-energy particles are trapped by it. References [3,4] give the details of the INC model used.

After the cascade an excited nucleus is formed that can again emit particles during the equilibrium process. The preequilibrium emission is described by the exciton model [43]. Its incorporation into the cascade calculations was presented in Ref. [40]. The thermalized nucleus can undergo multifragmentation at higher excitation energy or evaporate particles at lower energy [37]. After that, a residual nucleus remains which can be observed in the experiment.

Besides the preequilibrium emission, another effect which can also substantially decrease the excitation energy of the thermalized reaction product consists in the local density reduction during the process of cascade development, the so-called trawling effect [4,44]. Because of this effect, the number of collisions of the cascade particles inside the nucleus is decreased and hence the excitation energy of the residual nucleus is also decreased. The influence of this effect on the calculated mass yield distribution was also investigated.

The calculations were performed with the Monte Carlo method. Here 5000 antiproton annihilations were simulated for each of the theory versions listed below. Beta decay of the radioactive residual nuclei was not considered so that primary independent yields were obtained. The theory versions used were the following: (i) version 1, cascade without trawling + multifragmentation + evaporation; (ii) version 2, cascade without trawling + preequilibrium emission + multifragmentation + evaporation; (iii) version 3, cascade with trawling + multifragmentation + evaporation; and (iv) version 4, cascade with trawling + preequilibrium emission + multifragmentation + evaporation.

The same combinations of theory ingredients were also used to calculate the product yield of the interaction of 3.9 GeV protons with a  $^{nat}\text{Cu}$  target, a reaction used as reference throughout this paper. A comparison of the fitted experimental mass distribution with all four of the above versions of the theory is shown in Fig. 5. Clearly,

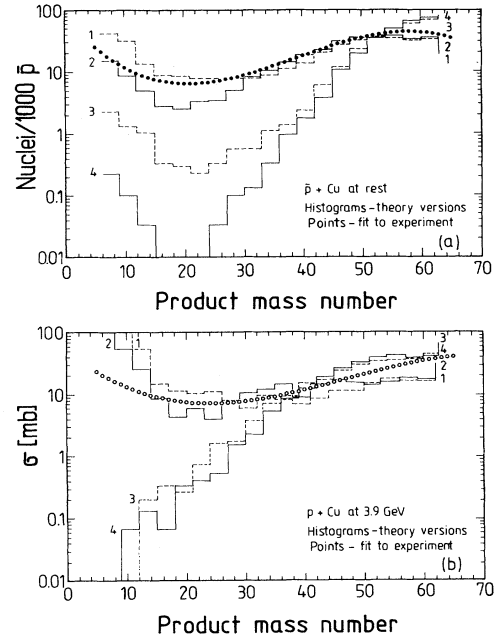


FIG. 5. Comparison of the fitted experimental mass distribution with four versions of the cascade plus evaporation model. The ingredients used in theory versions 1–4 are given in Sec. IV C.

the inclusion of the trawling effect is not supported by the experimental data on the mass yield in proton and antiproton reactions. Therefore, in Fig. 6, only versions of the theory without trawling are retained and are shown on an expanded scale. The deduced experimental yields for the measured  $A$  chains are also shown in this figure. The theoretical data for the individual, measured products are given in Table I for versions 1 and 2 of the theory.

At this point, one may conclude from Fig. 6 and Table I that the first two versions of the cascade model used give a fair account of the experimental mass yield in the proton-induced reactions and describe the antiproton data very well. Similarly, as was observed for previous antiproton data [7,8], the existence of the trawling effect is not supported by the mass yield data, and the necessity for the inclusion of the preequilibrium emission seems questionable. It should be pointed out, however, that one must be careful with the conclusions based only on a comparison of the isotope yield with the INC model. To make more definite conclusions, one needs to analyze the total set of experimental characteristics in the same framework.

As was shown in Refs. [4,44], it is important to take into account the trawling effect to describe the multiplicity of secondary protons and the correlations between the numbers of secondary protons and pions produced in the high energy ( $> 3$  GeV) proton-nucleus interaction and antiproton annihilation on nuclei. In particular, the tendency of the excitation energy to saturate and the number of knocked-out nucleons at the incident energy  $E_p \approx 3-5$  GeV is reproduced correctly by the INC model with trawling [44]. At the same time, the INC model without

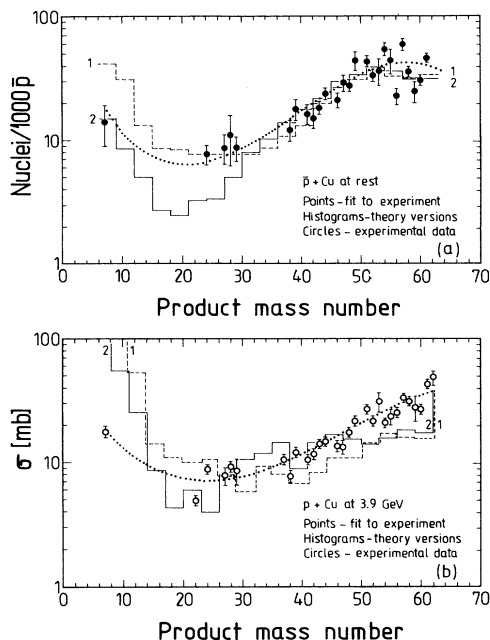


FIG. 6. Same as Fig. 5, but only for two theory versions which are closest to the experimental data. The experimental values gathered for each  $A$  chain are also shown.

trawling describes well the isotope yield. These results demonstrate some inconsistency of the INC model used.

At the present time, the INC model is the only model capable of calculating the distributions of nuclei in the excitation energy and mass. But there are serious oversimplifications in this model. First, this approach uses a Fermi-gas model to describe the target nucleus, and so the nucleus is excited by production of “holes” in the Fermi sea and excited nucleons above the Fermi level. This simple single-particle picture of the energy dissipation is not strictly correct. Second, the INC model does not take into account the production of mesonic and baryonic resonances and the hadronization length effects, which may be important at high incident energies. Also, the INC model with trawling uses the frozen nucleon ap-

proximation and so does not take into account the effects of relaxation of nuclear matter. This means that the INC model must be modified considerably to study the energy dissipation in high-energy nuclear reactions.

## V. SUMMARY AND CONCLUSIONS

In this work we have investigated the heavy reaction products issued from the interaction of stopped antiprotons with natural copper targets. The yield of the radioactive products was determined using gamma-ray spectroscopy techniques. From these data the charge dispersion and a complete mass yield distribution were deduced using a, by now, well-established minimization procedure. These distributions were compared with those gathered from pion and proton interactions with the same target.

The individual product yields as well as the complete mass distribution were compared with the intranuclear cascade plus evaporation model. A satisfactory agreement was obtained for a cascade version which does not include the trawling effect.

The most important message from the present work is that the tremendous energy available after antiproton annihilation is only in part stored in the nuclear system. In the Cu mass region, the average excitation energy of the system formed after the stopped antiproton annihilation seems to be similar, if not slightly lower, than after energetic ( $> 2$  GeV) proton interactions.

## ACKNOWLEDGMENTS

The competent cooperation of the LEAR staff during the irradiations is greatly appreciated. Our sincere thanks are due to Ludwik Pieńkowski for discussions and Weronika Płóciennik for the help in sample measurements and evaluations. This work was supported by Polish Grant No. 2 0210 91 01 from the State Committee for Scientific Research and by the German Bundesministerium für Forschung und Technologie, Bonn. One of us (H.S.P.) acknowledges support from a NATO Scientific Affairs Division grant.

- [1] J. Rafelski, Phys. Lett. **91B**, 281 (1980).
- [2] J. Rafelski, Phys. Lett. **B207**, 371 (1988).
- [3] A. S. Iljinov, V. I. Nazaruk, and S. E. Chigrinov, Nucl. Phys. **A382**, 378 (1982).
- [4] Ye. S. Golubeva, A. S. Iljinov, A. S. Botvina, and W. M. Sobolevsky, Nucl. Phys. **A483**, 539 (1988).
- [5] J. Cugnon and J. Vandermeulen, Ann. Phys. (Paris) **14**, 49 (1989).
- [6] E. F. Moser, H. Daniel, T. von Egidy, F. J. Hartmann, W. Kanert, G. Schmidt, M. Nicholas, and J. J. Reidy, Phys. Lett. **B179**, 25 (1986).
- [7] E. F. Moser, H. Daniel, T. von Egidy, F. J. Hartmann, W. Kanert, G. Schmidt, Ye. S. Golubeva, A. S. Iljinov, M. Nicholas, and J. J. Reidy, Z. Phys. A **333**, 89 (1989).
- [8] T. von Egidy, H. Daniel, F. J. Hartmann, W. Kanert, E. F. Moser, Ye. S. Golubeva, A. S. Iljinov, and J. J. Reidy, Z. Phys. A **335**, 451 (1990).
- [9] P. J. Karol, Phys. Rev. C **10**, 150 (1974).
- [10] J. B. Cumming, P. E. Haustein, R. W. Stoenner, L. Mautner, and R. A. Naumann, Phys. Rev. C **10**, 739 (1974).
- [11] J. B. Cumming, R. W. Stoenner, and P. E. Haustein, Phys. Rev. C **14**, 1554 (1976).
- [12] C. J. Orth, H. A. O'Brien, Jr., M. E. Schillaci, B. J. Drolepsky, J. E. Cline, E. B. Neischmidt, and R. L. Brodzinski, J. Inorg. Nucl. Chem. **38**, 13 (1976).
- [13] C. J. Orth, B. J. Drolepsky, R. A. Williams, G. C. Giesler, and J. Hudis, Phys. Rev. C **18**, 1426 (1978).
- [14] E. Hagebø, I. R. Haldorsen, M. B. Mostue, J. Pettersen, O. Scheidemann, T. Lund, L. C. Carraz, and C. Richard-Serre, Radiochim. Acta **35**, 133 (1984).
- [15] J. B. Cumming, P. E. Haustein, T. J. Ruth, and G. J. Virtes, Phys. Rev. C **17**, 1632 (1978).

- [16] J. B. Cumming, P. E. Hausteijn, and H.-C. Hseuh, *Phys. Rev. C* **24**, 2162 (1981).
- [17] D. G. Cole and N. T. Porile, *Phys. Rev. C* **24**, 2038 (1981).
- [18] T. Lund, D. Molzahn, R. Brandt, B. Bergersen, D. Erickson, E. Hagebø, I. R. Haldorsen, T. Bjørnstad, and C. Richard-Serre, *Phys. Lett.* **102B**, 239 (1981).
- [19] K. H. Hicks, T. E. Ward, M. Koike, and J. Peter, *Phys. Rev. C* **26**, 2016 (1982).
- [20] G. D. Cole and N. T. Porile, *Phys. Rev. C* **25**, 244 (1982).
- [21] T. Lund, D. Molzahn, B. Bergersen, E. Hagebø, I. R. Haldorsen, and C. Richard-Serre, *Z. Phys. A* **306**, 43 (1982).
- [22] L. Kowalski, P. E. Hausteijn, and J. B. Cumming, *Phys. Rev. Lett.* **51**, 642 (1983).
- [23] S. Y. Cho, Y. H. Chung, N. T. Porile, and D. J. Morrissey, *Phys. Rev. C* **36**, 2349 (1987).
- [24] S. Y. Cho, N. T. Porile, and D. J. Morrissey, *Phys. Rev. C* **39**, 2227 (1989).
- [25] L. Pieńkowski, J. Jastrzębski, W. Kurcewicz, A. Gizon, J. Blachot, and J. Crançon, *Phys. Rev. C* **43**, 1331 (1991).
- [26] P. E. Hausteijn and T. J. Ruth, *Phys. Rev. C* **18**, 2241 (1978).
- [27] C. J. Orth, W. R. Daniels, B. J. Dropesky, R. A. Williams, G. C. Giesler, and J. N. Ginocchio, *Phys. Rev. C* **21**, 2524 (1980).
- [28] S. Shibata, M. Imamura, T. Miyachi, M. Mutou, K. Sakamoto, Y. Hamajima, M. Soto, Y. Kubota, M. Yoshida, and I. Fujiwara, *Phys. Rev. C* **35**, 254 (1987).
- [29] V. B. Zlokazov, *Nucl. Instrum. Methods* **199**, 509 (1982); W. Karczmarczyk, M. Kowalczyk, and L. Pieńkowski (unpublished).
- [30] U. Reus and W. Westmeier, *At. Data Nucl. Data Tables* **29**, 2 (1983).
- [31] The ENSDF Radioactivity Data Base for IBM-PC and Computer Network Access, Peter Ekström and Leif Spanier, Department of Physics, Sövegaton 14, S-223 62 Lund, Sweden, August 1989.
- [32] W. Markiel, H. Daniel, T. von Egidy, F. J. Hartmann, P. Hofmann, W. Kanert, H. S. Plendl, K. Ziock, R. Marshall, H. Machner, G. Riepe, and J. J. Reidy, *Nucl. Phys. A* **485**, 445 (1988).
- [33] W. Skulski, B. Fornal, J. Jastrzębski, P. Koczoń, J. Kownacki, M. Opacka, T. Pawłat, L. Pieńkowski, W. Płóciennik, J. Sieniawski, P. P. Singh, J. Styczeń, and J. Wrzesiński, *Z. Phys. A* **342**, 61 (1992).
- [34] P. Jasselette, J. Cugnon, and J. Vandermeulen, *Nucl. Phys. A* **484**, 542 (1988).
- [35] P. Hofmann, F. J. Hartmann, H. Daniel, T. von Egidy, W. Kanert, W. Markiel, H. S. Plendl, H. Machner, G. Riepe, D. Protić, K. Ziock, R. Marshall, and J. J. Reidy, *Nucl. Phys. A* **512**, 669 (1990).
- [36] W. G. Lynch, *Annu. Rev. Nucl. Part. Sci.* **37**, 493 (1978).
- [37] A. S. Botvina, A. S. Iljinov, and I. N. Mishustin, *Nucl. Phys. A* **507**, 649 (1990).
- [38] W. A. Friedman, *Phys. Rev. C* **42**, 667 (1990).
- [39] L. G. Moretto, *Nucl. Phys. A* **247**, 211 (1975).
- [40] A. S. Iljinov, V. I. Nazaruk, and S. E. Chigrinov, *Nucl. Phys. A* **268**, 513 (1976).
- [41] V. S. Butsev, A. S. Iljinov, and S. E. Chigrinov, *Fiz. Elem. Chastits At. Yadra* **11**, 900 (1980) [*Sov. J. Part. Nucl.* **11**, 358 (1980)].
- [42] G. Rudstam, *Z. Naturforsch.* **A21**, 1027 (1966).
- [43] M. Blann, *Annu. Rev. Nucl. Sci.* **25**, 123 (1975).
- [44] V. S. Barashenkov, A. S. Iljinov, and V. D. Toneev, *Yad. Fiz.* **13**, 743 (1971) [*Sov. J. Nucl. Phys.* **13**, 422 (1971)].